Barotropic Decay of Baroclinic Waves in a Two-Layer Beta-Plane Model

STEVEN B. FELDSTEIN

Atmospheric and Oceanic Sciences Program, Princeton University, Princeton, New Jersey

ISAAC M. HELD

Geophysical Fluid Dynamics Laboratory/NOAA, Princeton University, Princeton, New Jersey

(Manuscript received 22 December 1988, in final form 24 May 1989)

ABSTRACT

A two-layer quasi-geostrophic model is used to study the effects of a meridionally sheared zonal flow on the life cycle of a weakly unstable baroclinic wave. In most of the cases analyzed, the fluid is inviscid with the exception of scale-selective fourth-order horizontal diffusion. The initial zonal flow is identically zero in the lower layer. The character of the eddy life cycle in the limit of weak supercriticality is shown to depend on whether or not the meridional shear in the upper layer is strong enough to produce a critical latitude for the wave.

If the shear is sufficiently weak, the wave undergoes periodic amplitude vacillation characterized by symmetric baroclinic growth and *baroclinic* decay. However, when the meridional shear is strong enough to allow for the existence of a critical layer, the flow undergoes an asymmetric life cycle which resembles that found by Simmons and Hoskins in a primitive equation model on the sphere: the wave grows baroclinically but decays *barotropically* toward a wave-free state. Throughout the barotropic decay stage, the wave is breaking and being absorbed either at or before the critical layer. As the supercriticality is increased, strong reflection begins to occur at the location of the wave breaking, resulting in irregular amplitude vacillation. Consistent with critical layer theory, when a reflecting state is created the solution is sensitive to the inclusion of higher zonal harmonics of the fundamental wave.

By relaxing the potential vorticity distribution back to an unstable state, periodic solutions are obtained in which each episode of growth and decay is similar to that found in these nearly inviscid solutions.

1. Introduction

An important feature of the observed life cycles of midlatitude synoptic-scale baroclinic waves is the asymmetry between growth and decay. The growth is primarily baroclinic; the decay barotropic. The eddies grow at the expense of the available potential energy of the mean flow, but the part of the eddy energy that is not dissipated is returned to the kinetic, rather than potential, energy of the mean flow during the decay phase.

Randel and Stanford (1985) describe a very clean example of this baroclinic wave life cycle in data from the Southern Hemisphere. Simmons and Hoskins (1978, 1980) provide a description of the asymmetry between growth and decay in their nonlinear integrations with a primitive equation model on the sphere. There is striking similarity between the results of Simmons and Hoskins, for a perturbation consisting of a single unstable zonal wavenumber and its harmonics, and the observational study of Randel and Stanford. The asymmetric life cycle is also captured in full general circulation models (GCMs), in the presence of forcing and dissipation. The first (two-level) primitive equation GCM on the sphere (Smagorinsky 1963) provides a particularly clear example. Our goal in this paper is to isolate the dynamics responsible for this asymmetry in as simple a context as possible.

Most analytical studies of weakly nonlinear baroclinic instability, primarily conducted with the quasi-geostrophic two-layer model, show waves undergoing a symmetric life cycle of baroclinic growth and baroclinic decay (Pedlosky 1970, 1971). The energy transferred to the eddy from the zonal available potential energy is returned to the zonal available potential energy during the decay stage. In these studies, the initial zonal mean flow is assumed to be independent of latitude. While meridionally sheared zonal flows are generated by the eddies as they evolve, for weakly unstable waves these shears are too small for the resulting barotropic conversions to compete in the wave energetics. In order that a simple analytical or numerical model represent the observed barotropic decay, it is clearly necessary that the basic state zonal flow vary both in the meridional and vertical directions.

Corresponding author address: Dr. Steven B. Feldstein, Department of Earth and Atmospheric Sciences, York University, 4700 Keele Street, North York, Ontario, Canada M3J 1P3.

Further clues as to the dynamics of this asymmetric life cycle are evident from the analysis of the Simmons–Hoskins calculations by Edmon et al. (1980) from the point of view of wave activity conservation and Eliassen–Palm (EP) fluxes (see also Held and Hoskins 1985). During the growth stage, the wave activity is propagating vertically, with the associated EP flux divergence providing acceleration of the zonal flow at low levels and deceleration at upper levels in midlatitudes. This vertical propagation implies that the energy conversions are predominantly baroclinic. During the decay stage, the wave activity propagates equatorward within the upper troposphere, so that the zonal flow is accelerated in midlatitudes and decelerated in the subtropics. Since the wave activity tends to be propagating horizontally at this stage, the meridional heat flux is small so that the energy conversions are primarily barotropic. At the end of the cycle, the mean flow has been modified by the irreversible mixing in two distinct regions: at low levels in midlatitudes, where the acceleration during the baroclinic growth stage persists; and in the subtropics at upper levels, where the deceleration occurs during the barotropic decay. In contrast, at upper levels in midlatitudes the flow is decelerated as the wave grows, but it is then returned to slightly larger than its original value as the wave radiates equatorward, with little irreversible mixing occurring (at least in these idealized calculations).

This analysis suggests that the irreversible mixing at upper levels is an essential aspect of the observed asymmetric life cycle. One can imagine that if the wave were reflected by a turning point or by a wall (in a channel model) without losing amplitude due to irreversible mixing, the propagation back to midlatitudes would reverse both the momentum fluxes and the associated barotropic conversion, leading to an energy cycle dominated by baroclinic conversions.

The mixing in the subtropical upper troposphere can be thought of as due to "wave breaking" (e.g., McIntyre and Palmer 1984) as the disturbance propagates into a region of smaller zonal winds. As long as a critical latitude exists in the upper troposphere, at which the zonal flow equals the wave's phase speed, such irreversible mixing is unavoidable, and a small incident disturbance will be at least partially absorbed (see Killworth and McIntyre 1985, for a review of critical layer theory). One is led to the hypothesis that the existence of a simple asymmetric life cycle of the sort found by Simmons and Hoskins could depend, in part at least, on the existence of an upper tropospheric critical layer.

Motivated by this picture we have examined the effects of different meridional shears on the life cycles of unstable baroclinic waves in a two-layer quasi-geostrophic, beta-plane channel model. We are particularly interested in finding basic flows for which a simple asymmetric life cycle similar to that seen by Simmons and Hoskins will occur in the two layer model. In particular, we compare flows in which meridional shear exists but is insufficient to produce an upper level critical layer with flows in which an upper level critical layer is present. Because of the complexity introduced by the critical layers, we use a numerical model rather than attempt an analytical weakly nonlinear theory.

Life cycles of baroclinic waves without upper level critical layers are examined in section 3. The case with strong meridional shear and upper level critical layers is discussed in section 4. Forcing and dissipation are added in section 5.

2. Model description

The two-layer model equations for a beta-plane can be written in dimensionless form as

$$\partial q_n/\partial t + J(\psi_n, q_n) = -\nu\nabla^6\psi_n, \tag{1}$$

where the subscript $n = 1$ corresponds to the upper layer and $n = 2$ the lower layer. The potential vorticities q_n are related to the streamfunctions ψ_n and the flow field through

$$q_n = \nabla^2\psi_n + \beta y + (-1)^n(\psi_1 - \psi_2)/2,$$
$$(u_n, v_n) = (-\partial\psi_n/\partial y, \partial\psi_n/\partial x). \tag{2}$$

Our notation follows Pedlosky (1987) except that the radius of deformation, λ, is chosen as the horizontal length scale, where

$$\lambda^2 = g(\rho_2 - \rho_1)H/(2\rho_2 f_0^2) \tag{3}$$

and H is the depth of either layer. The horizontal velocity scale is set equal to the maximum value of the initial upper layer zonal flow. The biharmonic horizontal diffusion is included to parameterize the enstrophy cascade to unresolved scales.

The streamfunctions ψ_n consist of a zonal mean plus a disturbance:

$$\psi_n(x, y, t) = \Psi_n(y, t) + \psi'_n(x, y, t);$$
$$U_n(y, t) = -\partial\Psi_n(y, t)/\partial y. \tag{4}$$

The initial value of the zonal flow is specified as

$$U_1(y, 0) = U(y); \quad U_2(y, 0) = 0, \tag{5}$$

where $U(y)$ reaches its maximum value of 1.0 and is symmetric about the center of the channel. The actual form of $U(y)$ will be presented later. The equation for the disturbance is

$$\partial q'_n/\partial t + U_n\partial q'_n/\partial x + v'_n\partial Q_n/\partial y + J(\psi'_n, q'_n) = -\nu\nabla^6\psi'_n, \tag{6}$$

where Q_n is the zonally averaged potential vorticity, and the corresponding equation for the zonal flow is

$$\partial Q_n/\partial t = -\partial(\overline{q'_n v'_n})/\partial y - \nu\nabla^6\Psi_n. \tag{7}$$

Calculations are performed both without the wave–wave interaction term $J(\psi'_n, q'_n)$ in (6) (the so called

quasi-linear or wave–mean flow interaction model) and with the term retained. When this term is set to zero, the disturbance is assumed to consist of only one zonal wavenumber.

The fluid is bounded at $y = 0$ and $y = W$ by rigid walls. Since the meridional velocity at the walls must vanish, it is necessary that

$$\partial\psi_n'/\partial x = 0 \quad \text{at} \quad y = 0, W, \tag{8}$$

and

$$\partial U_n/\partial t = -\nu\partial^4 U_n/\partial y^4 \quad \text{at} \quad y = 0, W. \tag{9}$$

Because of the presence of the higher-order derivative in the horizontal diffusion term, the boundary conditions

$$\partial\zeta_n'/\partial y = \partial^3\zeta_n'/\partial y^3 = \partial Z_n/\partial y = \partial^3 Z_n/\partial y^3 = 0, \tag{10}$$

where

$$\zeta_n' = \nabla^2\psi_n' \quad \text{and} \quad Z_n = \partial^2\Psi_n/\partial y^2 = -\partial U_n/\partial y, \tag{11}$$

are employed. Equations (8) and (9) are then consistently satisfied by requiring

$$\psi_n'(x, 0, t) = \psi_n'(x, W, t) = 0;$$
$$U_n(0, t) = U_n(0, 0) \quad \text{and} \quad U_n(W, t) = U_n(W, 0). \tag{12}$$

The numerical model chosen has equally spaced grid points in the meridional direction and an arbitrary number of waves in the zonal direction. The appropriate number of grid points is determined by gradually increasing the meridional resolution until the difference between successive solutions is negligible. The model equations are integrated in time with a leapfrog scheme. The effects of the computational mode are reduced by periodically restarting the model with the Euler-backward scheme. When more than one zonal wave is retained in the solution, the Jacobian is evaluated with the spectral transform method (Orszag 1970).

Given our nondimensionalization, the value of β is a measure of the supercriticality of the flow. The critical value below which instability occurs is denoted by β_c.

3. Weak shear

For our first example of a baroclinic eddy life cycle in a flow with meridional shear, we choose as an initial zonal wind profile

$$U_1 = 0.4 \sin(\pi y/W) + 0.6; \quad U_2 = 0, \tag{13}$$

which as is discussed below, does not produce an upper-layer critical level. The width of the channel W is set equal to 8.0. The horizontal diffusion coefficient is set to zero since there is no enstrophy cascade to small scales for this flow. The calculations in this section utilize 100 grid points between the channel walls.

A linear stability analysis was performed by integrating (6) with one zonal wavenumber retained while keeping the zonal mean terms fixed, until the disturbance settled into a normal model structure with a uniform phase speed and growth rate. The critical value of β was determined to be $\beta_c \approx 0.486$. The wave that first becomes unstable when β is slightly less than β_c has the zonal wavenumber $k = 0.78$ and the phase speed $c_r = 0.014$. This wave does not have a critical level; there is no point in the flow at which $U = c_r$, although $U - c_r$ is small throughout the lower layer.

We first ignore wave–wave interactions and examine the nonlinear evolution of the wave with the most unstable zonal wavenumber, $k = 0.78$, interacting with the zonal mean flow. The initial condition is the zonal flow (13) plus a very small eddy chosen to be symmetric about the center of the channel. The amplitude of the perturbation is sufficiently small that it settles accurately into the normal mode structure before nonlinearity becomes significant.

Choosing a small value of the supercriticality, $\beta = 0.4845$, the wave amplitude is found to be periodic, with a very long period of 1130. The energetics of this life cycle is shown in Fig. 1a. We see that the wave grows baroclinically and also decays baroclinically. The barotropic conversions are always 180 degrees out of phase with and smaller in magnitude than the baroclinic conversions. During the decay of the wave, the barotropic conversion is actually providing a source of eddy energy. This life cycle does not resemble those found in the more realistic models and in the observations discussed in the introduction. Except for the small barotropic conversions, these results resemble instead the two-layer analytical weakly nonlinear solution of Pedlosky (1970), where the wave undergoes a symmetric life cycle of baroclinic growth and decay. In Pedlosky (1982), the general form of the weakly nonlinear evolutionary equation of a baroclinic wave in a meridionally sheared zonal flow is determined when there is no critical layer present. Since the form of our initial zonal flow is the same as that in Pedlosky (1982), the same type of weakly nonlinear perturbative analysis would be valid for our problem for β slightly less than β_c. Although no explicit mention of energetics is made in Pedlosky (1982), a detailed examination would yield a life cycle that resembles Fig. 1a, with the baroclinic and barotropic conversions locked in phase relative to each other.

In Fig. 2 contours of streamfunction amplitude squared as a function of latitude and time are shown over one cycle of growth and decay. The meridional structure remains unchanged as the wave grows and decays, reflecting the symmetry of the energy conversions about the maxima in the eddy energy seen in Fig. 1a. In fact, the meridional variation of the streamfunction throughout the life cycle closely resembles that obtained from the linear stability analysis. This link between the linear and nonlinear solution is consistent

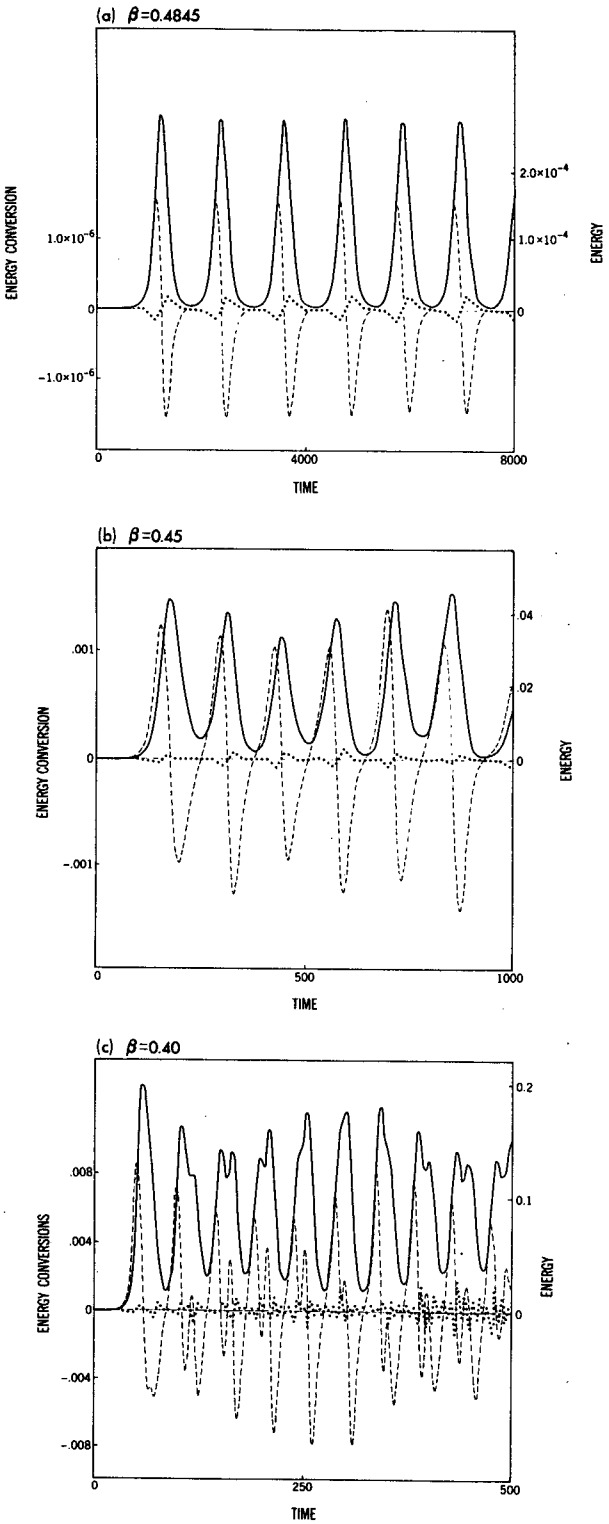

FIG. 1. Total energy and energy conversions as a function of time for the weak shear case (a) $\beta = 0.4845$, (b) $\beta = 0.450$, (c) $\beta = 0.400$. Solid line denotes total wave energy; dashed line, baroclinic energy conversion from the zonal flow to the wave; dotted line, barotropic energy conversion from the zonal flow to the wave.

with the weakly nonlinear results of Pedlosky (1982), where to lowest order in the expansion parameter, the meridional structure of the nonlinear solution is identical to the structure of the linear mode.

With a somewhat smaller value of $\beta = 0.45$, the amplitudes are larger and the flow appears to be aperiodic but the same type of life cycle occurs, with the baroclinic and barotropic conversions locked in phase (Fig. 1b). As β is reduced further, the flow develops in more complicated ways. At $\beta = 0.40$ (Fig. 1c), the baroclinic conversion still dominates, but now the barotropic conversions fluctuate at a higher frequency than the baroclinic conversions. All of these solutions are only weakly sensitive to the inclusion of higher zonal harmonics of the fundamental wave in the calculation. If eight zonal harmonics are retained, the same type of life cycles occur except that there is a

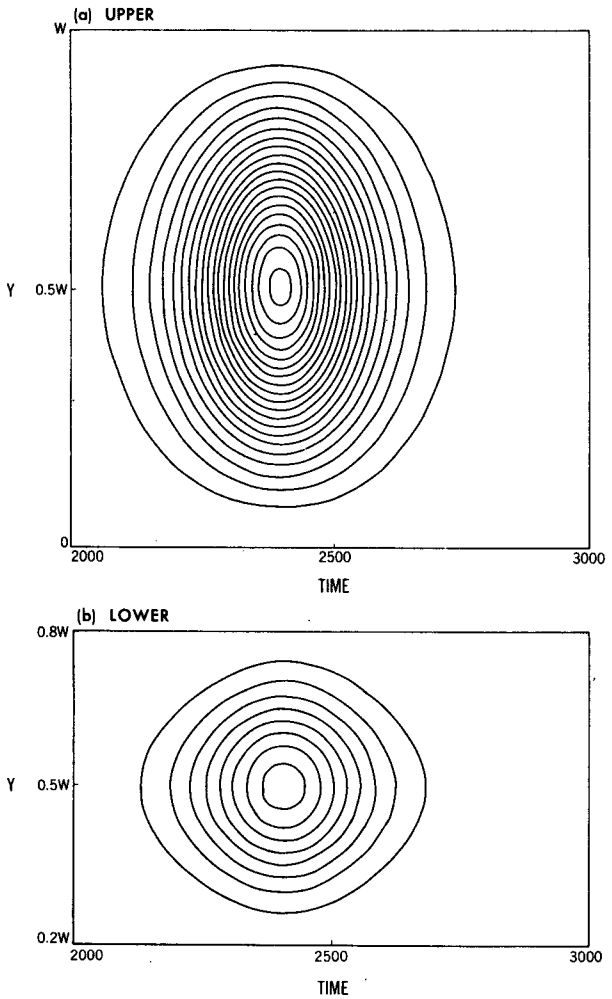

FIG. 2. Latitude–time contours of wave streamfunction squared for the weak shear case: (a) upper layer, (b) lower layer. Contour interval is 1×10^{-4} in (a), and 5×10^{-5} in (b).

small alteration in amplitude and period of the vacillation. As β is further reduced, the flow in the wave–mean flow calculation evolves in an irregular way with no apparent relationship between the sign or the magnitude of the energy conversions. However, these solutions are strongly sensitive to the presence of the higher harmonics.

4. Strong shear

As the meridional shear is increased in the flow (13) by increasing the constant multiplying $\sin(\pi y/W)$, and reducing the value of the additive constant so that $U(W/2, 0) = 1$, the character of the life cycle in the limit of weak supercriticality remains identical to that described in section 3, as long as the wave does not have a critical layer. When the shear is large enough that U_1 at the walls approaches zero and a critical layer is generated in the upper level, more complex behavior results. This particular flow does not generate a clean version of the desired asymmetric life cycle, partly because the presence of a wall very close to the critical layer modifies the reflection or absorption of wave activity by the layer, and partly because the initial unstable mode has significant amplitude at the critical layer. We find that a simpler life cycle is obtained when the critical layer is far removed from any boundaries and from the strongly unstable region itself. It also turns out to be helpful, as discussed further below, if the meridional shear is small at the critical layer. One initial zonal wind profile that satisfies these requirements is

$$U(y) = 0.2 + 0.8\exp[-(y - 0.5W)^2/\sigma_1^2] - 0.2\exp[-(y - 0.1W)^2/\sigma_2^2] - 0.2\exp[-(y - 0.9W)^2/\sigma_2^2], \quad \text{if} \quad 0.1W \leq y \leq 0.9W;$$

$$U(y) = 0, \quad \text{if} \quad 0 \leq y \leq 0.1W \quad \text{or} \quad 0.9W \leq y \leq W. \quad (14)$$

We choose $W = 40(2)^{1/2}$, $\sigma_1 = 0.05W = 2(2)^{1/2}$, $\sigma_2 = 0.2W = 8(2)^{1/2}$. The resulting wind profile is shown in Fig. 3a. We use 400 grid points within the domain. The choice of meridional resolution is determined by gradually increasing the number of grid points until the solution is essentially unchanged. The required resolution depends on the choice of the diffusion coefficient ν. For the following calculation we choose $\nu = 5 \times 10^{-5}$. As described below, this value of ν is large enough to dissipate small-scale eddies that are generated

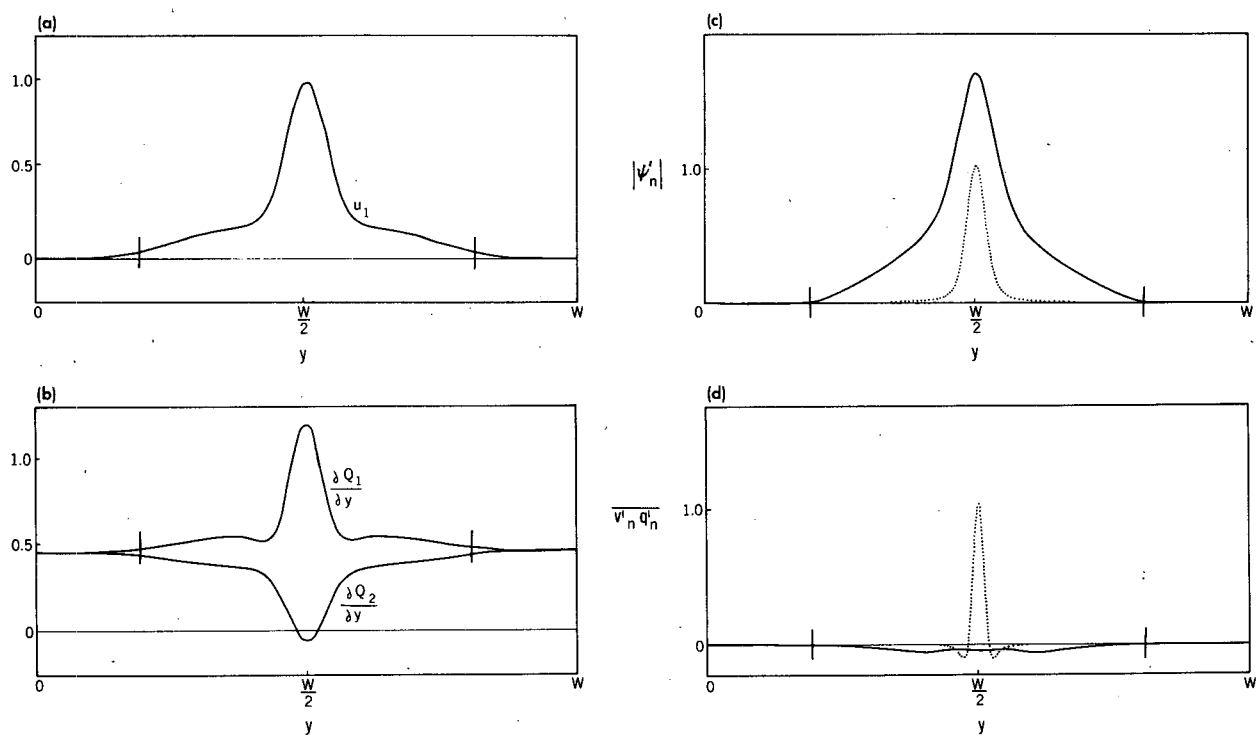

FIG. 3. (a) Initial upper level flow for the strong shear case with $\beta = 0.44$; (b) initial meridional potential vorticity gradients in the two layers; (c) magnitude of streamfunction for the unstable mode; and (d) potential vorticity flux in the unstable mode. The short vertical line denotes the location of the linear critical latitude. In (c) and (d), the solid line corresponds to the upper layer and the dotted line to the lower layer. The normal mode streamfunctions and fluxes are normalized by the values at the center of the channel in the lower layer.

in regions of Rossby wave breaking, but it is small enough so as to have a negligible effect on the larger-scale eddies outside these regions.

A linear stability analysis is performed for the zonal wind profile (14). Once again the procedure is to numerically integrate the linearized form of (6) until the perturbation settles into the fastest growing normal mode. This is done for increasingly larger values of β until $\beta = 0.45$ and the growth rate ω_i is less than 0.01. Calculations for smaller growth rates were not feasible because of the fine resolution required at the critical layer as the supercriticality goes to zero. Linear extrapolation was used to find β_c and c_r; the numerical integrations indicate that ω_i^2 and c_r both vary linearly with β at small supercriticalities. The extrapolation yields $\beta_c = 0.458$. For β slightly less than β_c the fastest growing normal mode has a zonal wavenumber $k = 0.82$ and $c_r = 0.013$.

a. *Weak supercriticality*

The initial meridional potential vorticity gradients are shown in Fig. 3b for a weakly supercritical case with $\beta = 0.44$. The critical layer for the unstable normal mode is also indicated. As for the flow considered in section 3, $\partial Q_1/\partial y$ is positive everywhere while $\partial Q_2/\partial y$ is negative in the center of the lower layer and positive elsewhere. Figures 3c and 3d show the linear normal mode streamfunction amplitudes and potential vorticity fluxes in the two layers. There is a large difference in structure between the two potential vorticity fluxes; the upper layer flux is broad whereas the lower layer flux is sharply confined to a narrow region consistent with the narrowness of the negative $\partial Q_2/\partial y$ region. Despite the broader structure in the upper layer, the amplitude of the upper layer streamfunction and the potential vorticity flux of the normal mode are essentially zero at the linear critical layer.

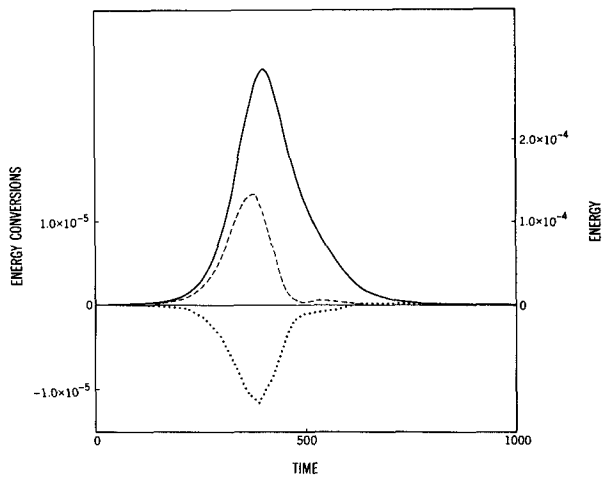

FIG. 4. Energy and energy conversions for the strong shear case when $\beta = 0.44$. Solid line denotes total wave energy; dashed line, baroclinic conversion; dotted line, barotropic conversion.

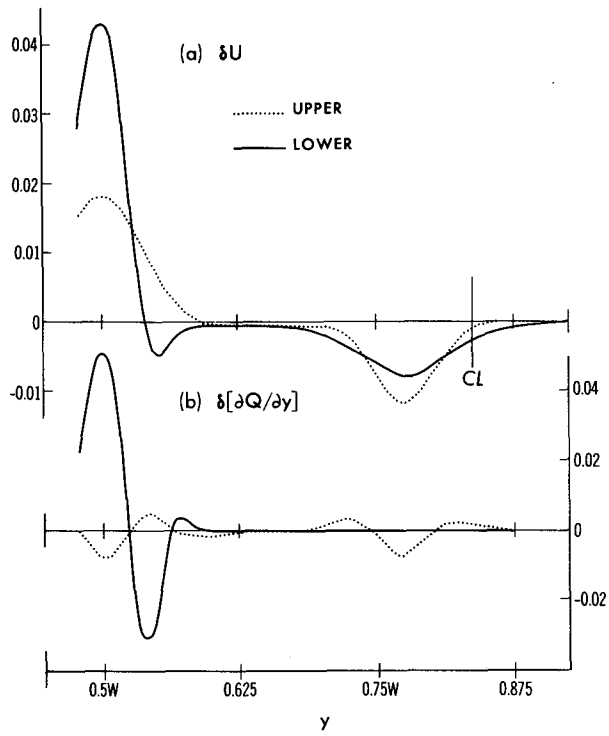

FIG. 5. The changes in (a) the zonal flow and (b) the potential vorticity gradients in the two layers resulting from the eddy life cycle with $\beta = 0.44$.

As in the weak shear case, we first truncate the unstable wave to one zonal wavenumber and then check if the results are sensitive to the inclusion of higher harmonics. With $\beta = 0.44$, the wave undergoes only one cycle of baroclinic growth followed by barotropic decay, as shown in Fig. 4. The final state is wave free. This energy cycle is in qualitative agreement both with the more complex numerical models and with the observational studies discussed in the Introduction, and is clearly distinct from the symmetric growth and decay described in section 3. The evolution is extremely slow by atmospheric standards, because of the very weak supercriticality.

The changes in U_n and $\partial Q_n/\partial y$ by the end of the life cycle are shown in Fig. 5. We see that U_n undergoes changes in two distinct regions. In the center of the channel, where the baroclinicity is largest, the zonal wind has increased slightly in the upper layer and more strongly in the lower layer. On the wings of the profile, where the baroclinicity is very small, the zonal wind has been decelerated in both levels, with the largest changes in the upper level, near the location of the linear critical latitude. The changes in $\partial Q_n/\partial y$ are even simpler: in the region of strongest baroclinicity, by far the largest changes in the potential vorticity gradient

are in the lower layer; near the critical latitude the gradient is changed only in the upper layer. The modification in the lower layer has rendered the flow stable; as indicated in Fig. 6, $\partial Q_2/\partial y$ is now positive everywhere. (As β is lowered, the region of negative $\partial Q_2/\partial y$ first appears at $\beta = 0.5$. Since β_c is significantly less than 0.5, or equivalently there exists a broad region of strongly negative $\partial Q_2/\partial y$ values, it is surprising that such a weakly supercritical wave is able to destroy the region of negative $\partial Q_2/\partial y$ so thoroughly.)

The changes in U_n and $\partial Q_n/\partial y$ are related to the eddy potential vorticity fluxes by

$$\partial U_n/\partial t = \overline{v_n' q_n'} + v_n^* \tag{15}$$

$$\partial(\partial Q_n/\partial y)/\partial t = -\partial^2(\overline{v_n' q_n'})/\partial y^2, \tag{16}$$

where v_n^* is the "residual" meridional circulation that satisfies

$$\partial^2 v_n^*/\partial y^2 - 2v_n^* = (-1)^n(\overline{v_2' q_2'} - \overline{v_1' q_1'}). \tag{17}$$

Near the critical latitude, the upper layer potential vorticity flux directly decelerates the upper layer winds and induces a residual circulation that decelerates the lower layer and reduces the deceleration in the upper layer by the same amount. In the same way, the residual circulation near the center of the channel redistributes some of the mean flow acceleration from the lower to the upper layer.

The deceleration of U_1 and the reduction of $\partial Q_1/\partial y$ in the upper layer clearly cannot be accounted for by the normal mode structure. Figure 7 shows the evolution of the streamfunction amplitude squared and potential vorticity flux in the two layers through the life cycle. The upper level streamfunction (7a) spreads laterally as the mean flow in the center of the domain is stabilized; while there is little change from the normal mode structure in the lower layer (7b). The structure of the upper-layer potential vorticity flux (7c) initially resembles that of the linear solution but then deviates strongly. It changes sign at about the time of maximum eddy energy, but there is no accompanying change in sign of this flux farther away from the middle of the channel. The potential vorticity flux near the linear critical latitude is always negative. In the lower layer, the structure of the potential vorticity flux is much simpler, as it is essentially confined to the negative $\partial Q_2/\partial y$ region and is everywhere positive.

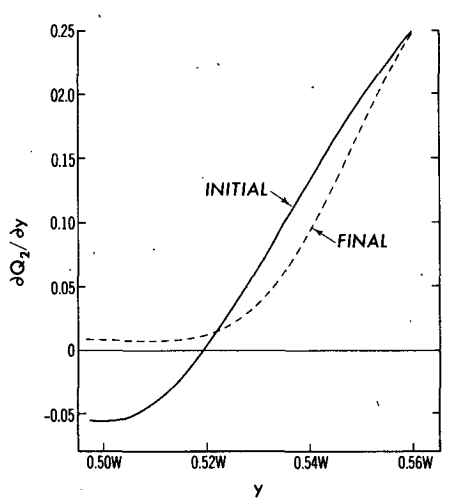

FIG. 6. The initial and final potential vorticity gradient in the lower layer near the center of the channel with $\beta = 0.44$.

The poleward heat flux (not shown) is nearly identical in structure to the potential vorticity flux in the lower layer, indicating that the momentum fluxes are essentially confined to the upper layer, consistent with the fact that little latitudinal dispersion can be seen in Fig. 7b. The momentum flux in the upper layer is shown in Fig. 7e. The convergence into the center as the wave begins to radiate outwards evolves into a pattern with strong divergence from the vicinity of the critical latitude. The energy equations for the two-layer model are

$$dE/dt = -0.5 \int dy \overline{v_1'(\psi_1' - \psi_2')}(U_1(y,t) - U_2(y,t)) - \int dy \overline{v_1' \zeta_1'} U_1(y,t) - \int dy \overline{v_2' \zeta_2'} U_2(y,t). \tag{18}$$

Since both $\overline{v_2' \zeta_2'}$ and $U_2(y)$ are small, the barotropic conversion in the lower layer is negligible. As the disturbance evolves from its linear structure, the upper layer vorticity flux increases relative to the heat flux, as is reflected in the change in sign of the upper-layer potential vorticity flux at the center of the channel. Because of this change in the ratio of the two fluxes during the nonlinear evolution of the wave, the barotropic conversion eventually dominates and the wave decays barotropically. The dissipation that occurs as the wave approaches its critical latitude then ensures that the decay is irreversible.

Except for the fact that the present β-plane results are symmetric about the jet center, the life cycle obtained is qualitatively similar to that of Simmons and Hoskins (1978; as analyzed further in Edmon et al. 1980). It is the spherical geometry in their calculations that creates a preference for equatorward propagation and poleward momentum flux during the barotropic decay. This effect of sphericity on the asymmetry of the eddy momentum fluxes has been examined by Williams (1988). He finds that the time-averaged eddy momentum fluxes are symmetric if the jet is sufficiently narrow. In this case, the variation of β is small both over the region of wave growth and over the broader

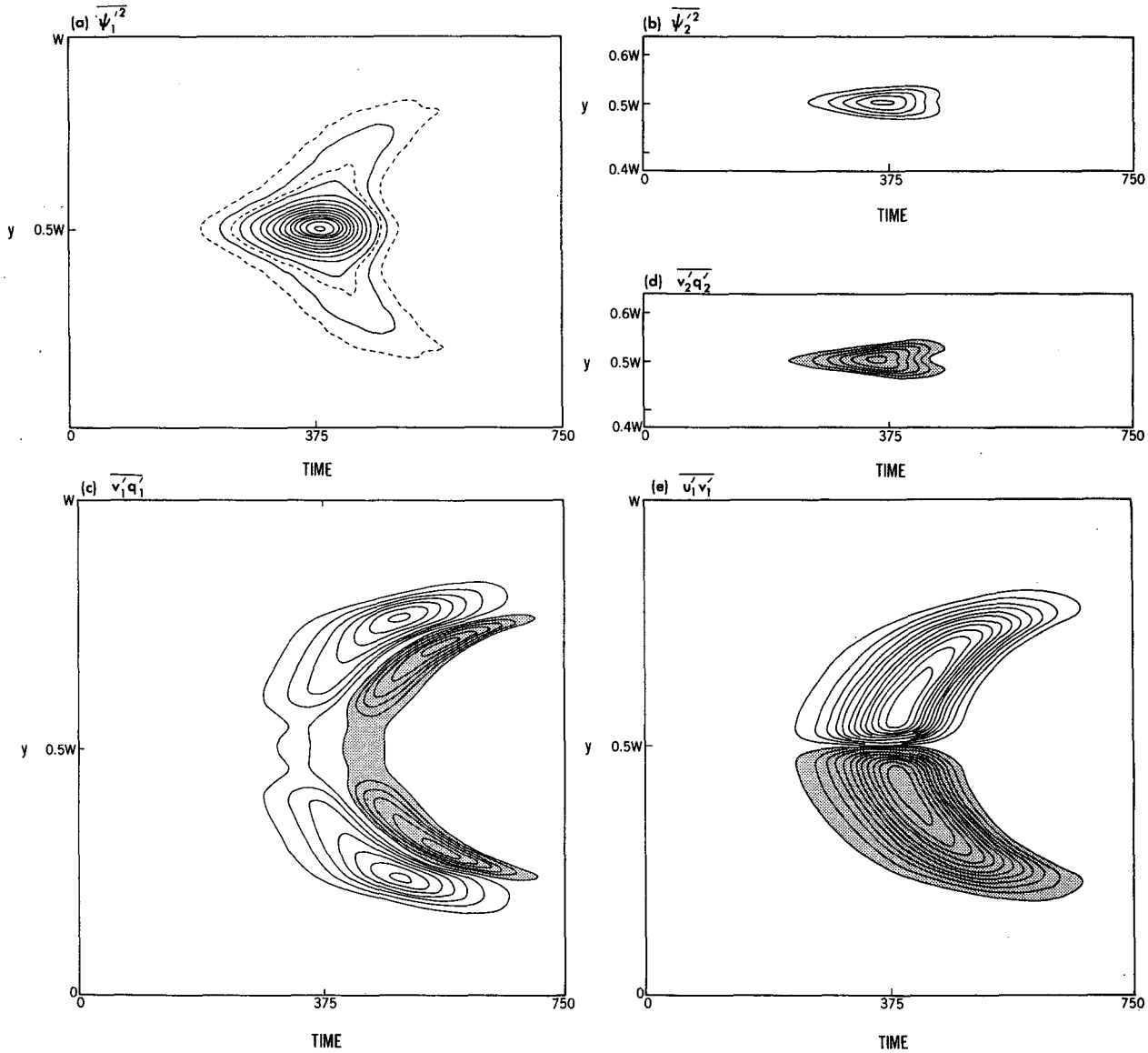

FIG. 7. Latitude–time contour diagrams for the strong shear case when $\beta = 0.44$: (a) $\overline{\psi_1'^2}$, contour interval 2.5×10^{-4}; (b) $\overline{\psi_2'^2}$, interval 2.5×10^{-4}; (c) $\overline{v_1'q_1'}$, interval 2.5×10^{-5} with values greater than 4.0×10^{-5} stippled; (d) $\overline{v_2'q_2'}$, interval 1.0×10^{-4} with values greater than 1.0×10^{-4} stippled; (e) $\overline{u_1'v_1'}$, interval 4.0×10^{-5} with values greater than 4.0×10^{-5} stippled. The zero contour has been omitted in (c)–(e).

region of wave radiation. On the other hand, for baroclinic jets that are wide enough to allow for a significant variation of β, the momentum fluxes are strongly asymmetric.

The change in U_1 and $\partial Q_1/\partial y$ near the linear critical layer are consistent with the ideas of linear critical layer absorption. The potential vorticity gradient in this region has only been modified slightly; given the width of the region in which U_1 is decelerated the wave does not have sufficient amplitude to generate a nonlinear, reflecting critical layer (e.g., Geisler and Dickinson 1974; Beland 1976; Warn and Warn 1978). We have checked to see how the dominant phase speed of the disturbance changes during the life cycle by examining the change in phase of q_1 from one time step to the next, averaging over all grid points in the center of the channel. It is found that the phase speed of the wave remains close to its linear value of 0.022 throughout the life cycle, verifying that the mean flow deceleration in the upper layer occurs near the waves critical level.

We also find that the center of the upper layer deceleration shifts closer to the critical layer as the diffusivity is lowered.

b. Moderate supercriticality

The energy cycle for a somewhat more supercritical flow, with $\beta = 0.38$, is shown in Fig. 8. The disturbance still undergoes a life cycle of baroclinic growth followed by barotropic decay to a wave free-state, but there are now small amplitude oscillations that take place prior to the final wave decay. The corresponding evolution of the upper layer streamfunction amplitude and potential vorticity flux are shown in Fig. 9. The outward radiation is less evident than in the more weakly supercritical case, and the potential vorticity fluxes develop similar structures but closer to the jet center. Consistently, the deceleration of the upper level zonally averaged flow and the changes in $\partial Q_1/\partial y$ (Fig. 10) are largest close to the channel center, although there is still a broad deceleration that extends outwards to the critical latitude.

We compute that the dominant phase speed in the flow evolves from its linear value of 0.057 up to 0.075 at the end of the life cycle. Despite this increase, the dominant phase speed is always less than the upper-layer zonal flow speed in the region of largest mean flow modification. One can describe the wave as breaking well before it reaches its critical layer. The process can be seen in the upper layer potential vorticity maps in Fig. 11. The first panel (a) shows the linear growth stage, where the particle displacements increase with time but maintain the same meridional structure. The disturbance only travels a short distance until the potential vorticity contours overturn and the wave breaks (b). Part of the disturbance then propagates further until it too breaks (c). Eventually there are breaking

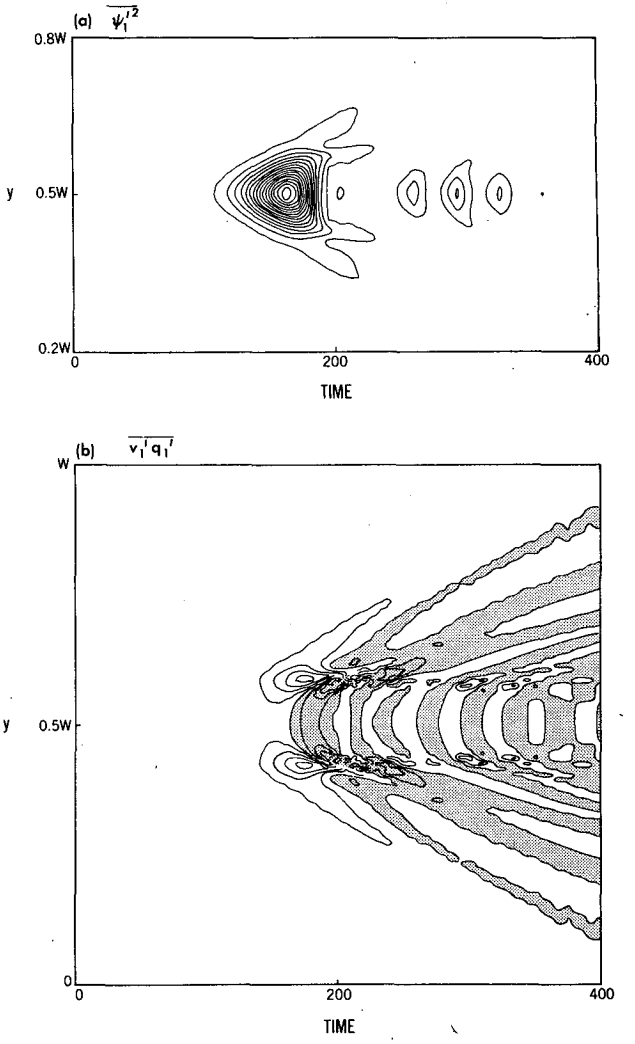

FIG. 9. Latitude–time contour diagrams in the strong shear case when $\beta = 0.38$: (a) $\overline{\psi_1'^2}$, interval is 7.5×10^{-3}, (b) $\overline{v_1'q_1'}$, interval 1.25×10^{-3}. Stippled regions are positive.

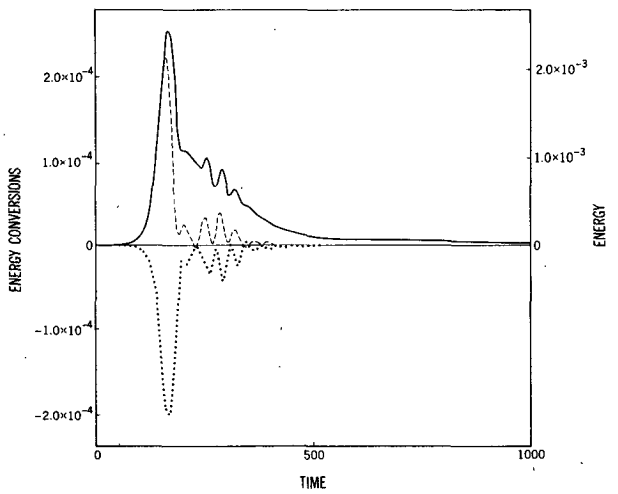

FIG. 8. As in Fig. 4, except $\beta = 0.38$.

waves extending all the way to the linear critical layer. At the last stage (d), the waves breaking at the linear critical layer are dissipated away. The problem of determining when a Rossby wave will break far from its critical latitude, and what the resulting pattern of mean flow deceleration will be, is an intriguing one that can be addressed with barotropic models of the sort discussed by Held and Phillips (1987).

The change in the upper level flow due to the eddy life cycle are compared in Fig. 12 for four different values of the supercriticality. As β is reduced from 0.44, the region of deceleration near 0.75°W gradually broadens and shifts towards the jet center. However, a distinct region of wave breaking and deceleration emerges at $\beta = 0.40$, and dominates the picture at $\beta = 0.38$.

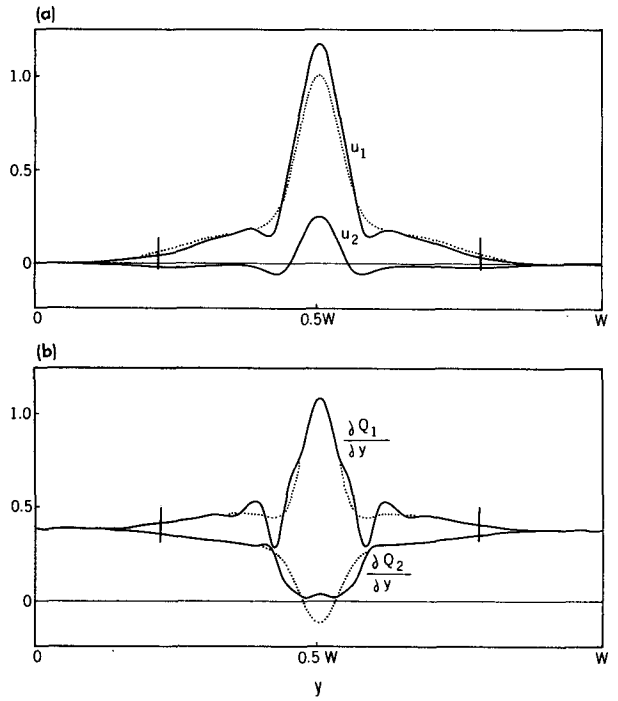

FIG. 10. The initial and final zonal flows and potential vorticity gradients, with $\beta = 0.38$. Dotted line denotes initial flow; solid line, final flow.

The upper-layer momentum fluxes associated with the outward wave radiation are upgradient and thus generate the barotropic decay. But it is the irreversible mixing due to wave breaking rather than the barotropic decay per se that is responsible for the simple life cycle leading to a wave-free state. We have modified the initial zonal flow in (14) by increasing the value of the upper layer wind far from the channel center so that a critical latitude is no longer present. In the limit of weak supercriticality, a symmetric life cycle of baroclinic growth and decay occurs just as in section 3. For larger supercriticalities, the structure of the disturbance evolves as it radiates outward, decaying barotropically in the process. It then reflects off the walls and returns to channel center again. A complicated life cycle represented by episodes of barotropic growth and decay results.

c. *Strong supercriticality*

All of the solutions described above are only weakly sensitive to the inclusion of higher harmonics of the fundamental unstable wave. Both the amplitude of the disturbance and the length of time over which the decay occurs change slightly. However, the sensitivity to the inclusion of higher harmonics increases when β is lowered further. We describe results for $\beta = 0.34$. In the one-wave calculation, instead of undergoing one major cycle of growth and decay, the disturbance maintains itself through a complex process of irregular baroclinic and barotropic conversions. The upper layer mixing is sufficient to generate negative values of $\partial Q_1/\partial y$. The sign of $\partial Q_1/\partial y$ oscillates in time, and there is a simultaneous alternation in sign of the upper-layer potential vorticity flux at the same location. This behavior is analogous to that in a quasi-linear critical layer, as described by Haynes and McIntyre (1987), in which the changes in sign of the potential vorticity gradient are associated with an oscillation between absorbing and overreflecting states.

Haynes and McIntyre show that this behavior is modified as more harmonics of the fundamental wave are added to the model. Consistent with their analysis, we find that a fully nonlinear calculation produces a simpler evolution towards a wave free-state, presumably because the fully nonlinear model tends to evolve towards a perfectly reflecting state without exhibiting periods of strong overreflection. Figure 13 compares the evolution of the wave energetics for the one wave case with that for a solution with 4 waves—the unstable wave and its first three harmonics. (The addition of more waves produces insignificant changes in this plot). The potential vorticity contours (not shown) evolve into localized vortex streets (lines of closed potential vorticity contours) in the region where $\partial Q_1/\partial y$ is small.

d. *Sensitivity to diffusion coefficient*

Recalling that in all previous calculations $\nu = 5 \times 10^{-5}$, the calculations with $\beta = 0.44$ and 0.38 were redone after increasing and decreasing the value of ν. The same life cycle characterized by baroclinic growth and barotropic decay still occurs, but there is some dependence on ν. When $\nu = 5 \times 10^{-6}$, the solutions are similar except that the disturbance decays a bit more slowly and the potential vorticity contours wrap around more extensively. When $\nu = 5 \times 10^{-4}$ the opposite is true. Also, for the smaller value of ν, there is essentially no difference in the zonally averaged flow in the center of the channel, whereas for values as large as 5×10^{-4} one begins to find significant changes.

The width of the region in which the upper level flow is decelerated is important for the character of the life cycle. As ν is lowered, we find that the center of the deceleration shifts slowly towards the critical layer, but its width does not decrease noticeably. If we fix the amplitude at which the unstable wave equilibrates near the center of the channel, or, more precisely, the amount of pseudomomentum (or wave activity) that radiates outwards to the region of wave breaking, then the zonal flow change, integrated over the breaking region, is also fixed. The narrower this region, the larger the local deceleration, and the greater the modification to the potential vorticity gradient. Only if this region is sufficiently wide will the modification to the potential vorticity gradient be small enough for linear critical

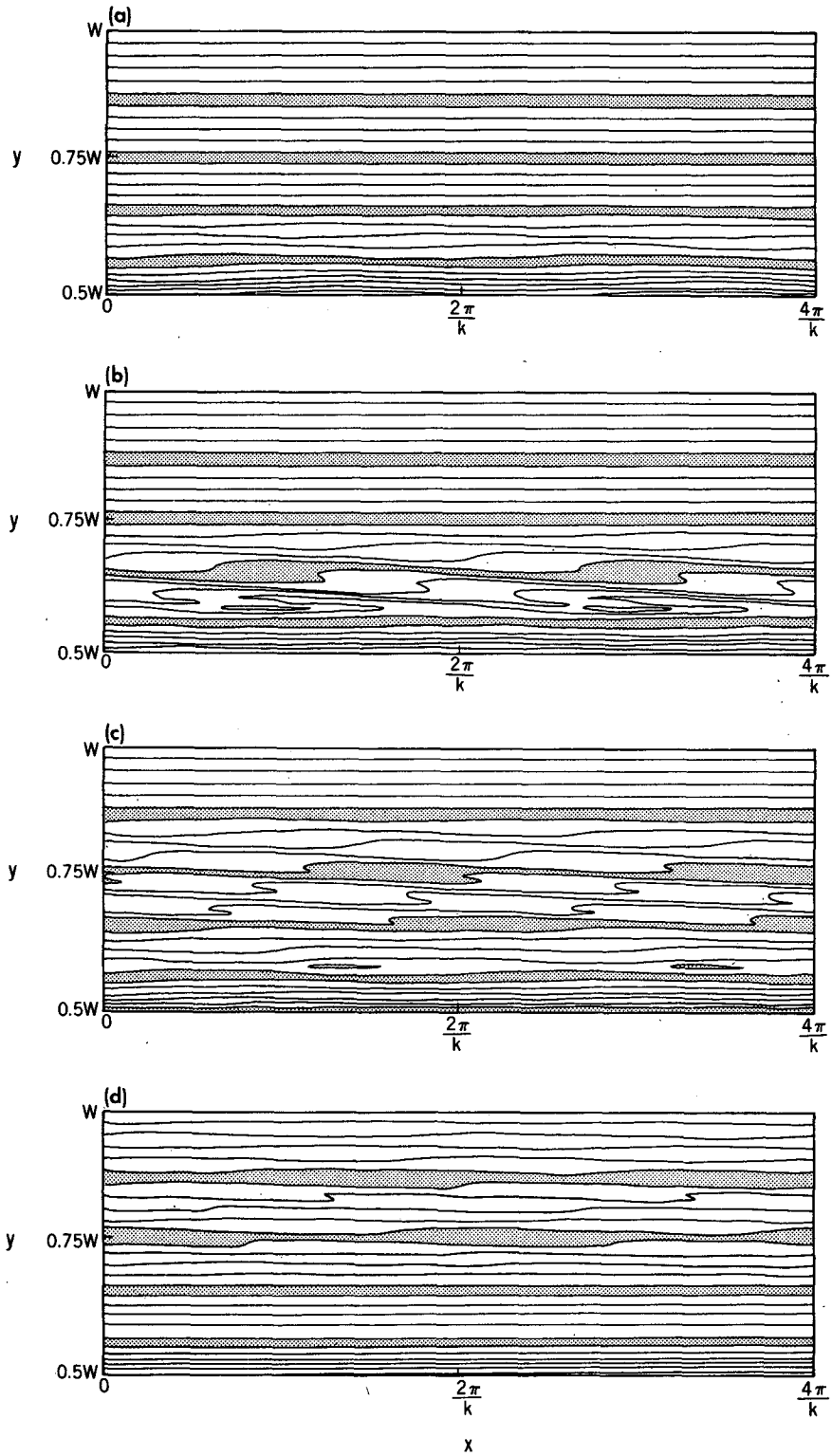

FIG. 11. Contours of absolute potential vorticity in the upper layer when $\beta = 0.38$ (a) $t = 175$, (b) $t = 200$, (c) $t = 300$, (d) $t = 450$.

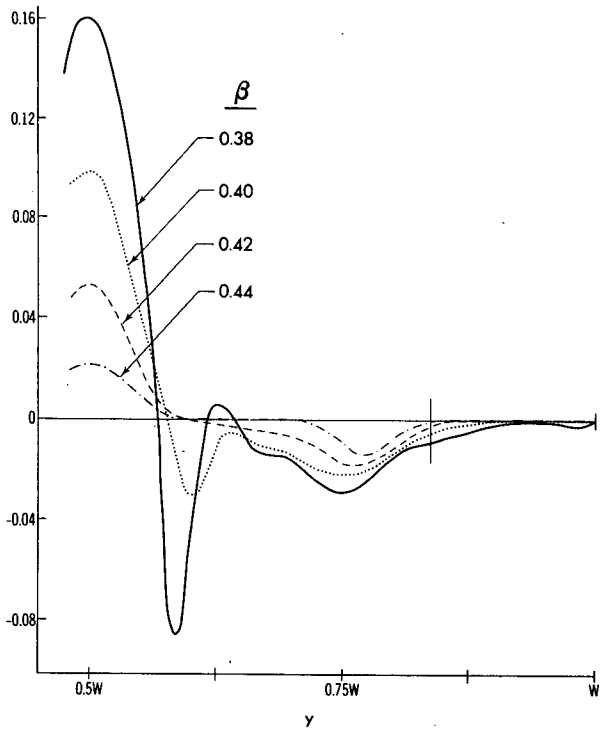

FIG. 12. Changes in the upper zonal flow for different values of β.

layer theory to be valid, resulting in strong wave absorption and the simple life cycle portrayed in Fig. 4.

Our calculations are in the regime where the diffusivity has little effect on the width of the critical layer absorption. In the limit of vanishing diffusivity, linear theory predicts that the width of the critical layer, or breaking region is

$$L_c = \Delta c/(\partial U/\partial y)_{\text{C.L.}}, \qquad (19)$$

where $(\partial U/\partial y)_{\text{C.L.}}$ is the meridional shear at the critical layer and Δc is the width of the phase speed spectrum of the incoming disturbance. We do not fully understand how Δc is determined, but presume that the imaginary part of the phase speed of the unstable normal mode is relevant.

e. *Gaussian profile*

Calculations have also been performed with the simpler Gaussian initial wind profile:

$$U(y) = \exp[-(y - 0.5W)^2/\sigma_1^2], \qquad (20)$$

with $\sigma_1 = 0.05W = 2(2)^{1/2}$ as before. Compared with the flow (14), the most important difference appears to be that the meridional shear at the critical latitude for the unstable mode on the flow (20) is much larger. As described above, given the incoming disturbance, this will result in a narrower region in which the mean flow is decelerated near the critical layer and larger changes in the potential vorticity gradient, making it harder to produce an absorbing layer. Consistent with this picture, we find that even smaller supercriticality is needed with the Gaussian jet in order to produce a simple life cycle that exhibits a single episode of baroclinic growth, followed by barotropic decay to a wave-free state. As an example, the evolution with $\beta = 0.44$ results in a mean flow modification comparable to that obtained with $\beta = 0.38$ in Fig. 9. (The change in β_c is very small.) Also, because the critical layer is closer to the baroclinically active zone, it is more difficult to separate the mean flow deceleration directly associated with the critical layer from that related to finite-amplitude wave-breaking at the jet margins of the sort seen in Fig. 11. It is for these reasons that we concentrate instead on results from the somewhat contrived Gaussian profile with wings.

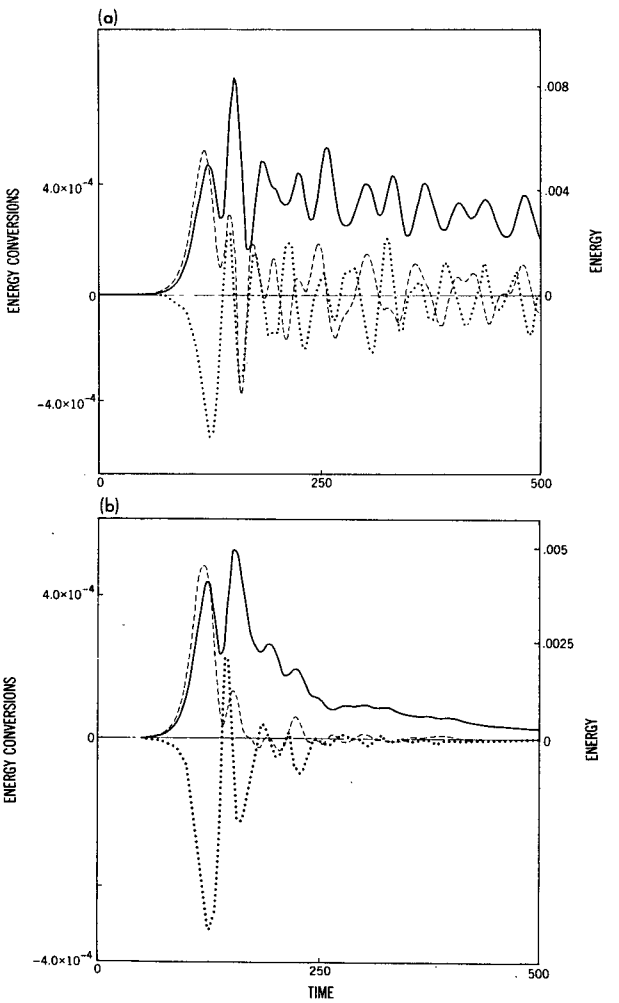

FIG. 13. Energy and energy conversions for the strong shear case when $\beta = 0.34$ (a) one zonal wavenumber solution, (b) four zonal wavenumber solution.

5. Life cycles with forcing and dissipation

In this section, we demonstrate that similar life cycles can be obtained in a model with forcing and dissipation. We choose to force the system in the simplest possible way by relaxing the flow towards its "radiative equilibrium" with potential vorticity damping of equal strength in the two layers. The potential vorticity equation with forcing and damping terms present, is now written as

$$\partial Q_n/\partial t + J(\psi_n, Q_n) = -\nu\nabla^6\psi_n - r(Q_n - Q_n^*), \quad (21)$$

where $Q_n^*(y)$ describes the radiative equilibrium profile. Both weakly sheared and strongly sheared zonal flows, with Q_n^* consistent with (13) and (14) respectively, have been examined.

For the weak shear case, we describe only the weakly supercritical cases with $\beta = 0.44$, for which the model's behavior is very simple: the disturbance evolves to a steady state for all nonzero values of r examined (down to values as small as 0.0001). In this steady state, the balance is primarily between the baroclinic energy conversion and dissipation.

The life cycles in the strong shear case depend upon the value of r. As an example, when $r = 0.028$ and $\beta = 0.32$ (see Fig. 14), we find that the solution is periodic. The wave growth is baroclinic but the decay is due to a combination of barotropic conversion and dissipation. During the early part of the decay stage, the barotropic conversion is the one with the largest magnitude. Thus, the disturbance undergoes a succession of individual life cycles characterized by baroclinic growth followed by barotropic decay.

In Fig. 15, the zonally averaged flow is shown both at the beginning and at the end ($t = 250$) of an individual growth and decay cycle. The modification to U_n and $\partial Q_n/\partial y$ is similar to the $\beta = 0.38$ inviscid solution in that the deceleration is localized at the margins of the jet, but there is little evidence of the broader deceleration in the wings of the profile extending towards the critical latitude. The tendency to break at the jet margins at this supercriticality, combined with the effect of the damping, prevents the wave from radiating as far from the generation region as the weakly nonlinear inviscid solution in Fig. 7. In the plot of the potential vorticity flux in Fig. 16, one sees the upper

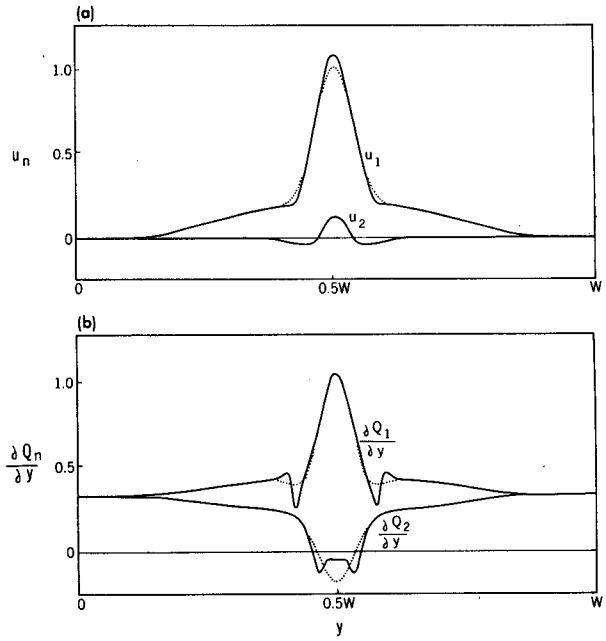

FIG. 15. Zonal flows and potential vorticity gradients before (dotted) and after (solid) an eddy event, with $\beta = 0.32$ and $r = 0.028$.

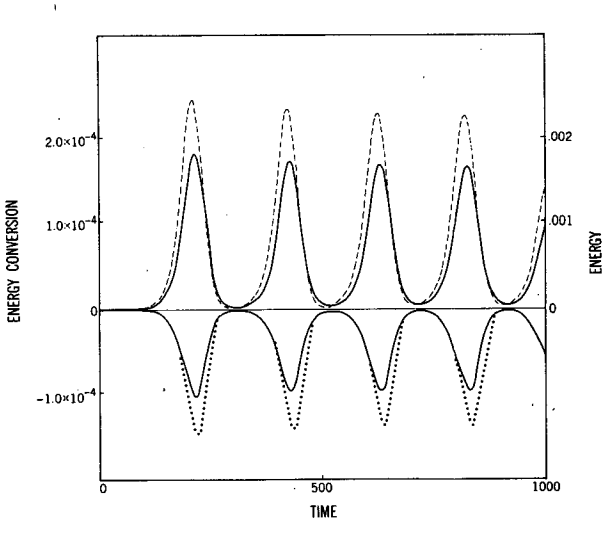

FIG. 14. Energy conversions, total energy, and energy lost to potential vorticity damping when $\beta = 0.32$ and $r = 0.028$. Solid line above the axis denotes total wave energy; dashed line, baroclinic conversion; dotted line, barotropic conversion; solid line below the axis, potential vorticity damping.

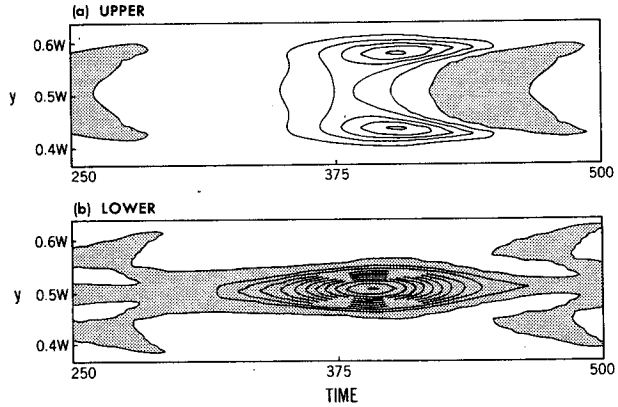

FIG. 16. Latitude–time contour diagrams in the strong shear case when $\beta = 0.32$ and $r = 0.028$: (a) $\overline{v_1'q_1'}$, interval is 1.0×10^{-3}; (b) $\overline{v_2'q_2'}$, interval 1.0×10^{-3}. Stippled regions are positive.

layer flux evolves from a structure that closely resembles that of the linear normal mode, toward a structure consistent with the localized deceleration away from the jet center, roughly as in the moderately supercritical inviscid solution described in section 4. The evolution of the lower layer flux more closely resembles that of the inviscid solution.

After the barotropic decay to a nearly wave-free state, the forcing restores the unstable mean flow, and the process is repeated. This qualitative behavior seems to be present for a range of values of r, no matter how small the supercriticality.

As r is increased for fixed supercriticality, the periodic solution is eventually replaced by a steady one. As in the weak shear case, the steady state consists of a balance between a positive baroclinic conversion and dissipation.

6. Summary and conclusions

The effect of different meridionally sheared zonal flows on the life cycles of baroclinic waves is examined with a two-layer quasi-geostrophic model. When the flow is weakly supercritical, it is found that the most important factor that influences these life cycles is whether or not the meridional shear is strong enough to create a critical latitude in the upper layer.

When there is no critical latitude present, the disturbance undergoes a symmetric life cycle of baroclinic growth followed by baroclinic decay. On the other hand, when there is a critical latitude present, an asymmetric life cycle of baroclinic growth and barotropic decay occurs. This asymmetric life cycle resembles those observed in the atmosphere (Randel and Stanford 1985) and in multilevel primitive equation models (Simmons and Hoskins 1978, 1980).

In the weak shear case, the meridional structure of the disturbance retains its linear form throughout its life cycle. However, in the strong shear (critical latitude) case, the meridional structure of the disturbance undergoes drastic changes with time, no matter how small the supercriticality. This result implies that a weakly nonlinear perturbative analysis with a single dominant normal mode can be performed for the weak shear case, but not for the strong shear case.

These changes in structure associated with outward radiation are clearly essential if the barotropic conversion is to increase relative to the baroclinic conversion until barotropic decay occurs, but a cascade to small scales, "wave breaking," is then required to make this decay irreversible and allow the evolution towards a wave-free state. The location of the Rossby wave breaking is close to the linear critical latitude if the supercriticality is exceedingly small. But as the wave amplitude increases, breaking becomes a possibility far from the critical latitude. This fact suggests that the critical latitude is not really the essential element; what is essential is the wave breaking that results in efficient absorption of the radiating waves and prevents their return to the region of strong baroclinicity. The critical latitude is important in that it causes waves of arbitrarily small amplitude to break.

The qualitative character of the flow evolution depends on whether the resulting mixing is sufficient to destroy the mean potential vorticity gradients. If it is not, and significant gradients remain, the breaking layer will be absorbing and relatively simple evolution towards a wave-free state is possible. If the gradients are destroyed, the wave can overreflect and an irregular life-cycle ensues. The wave amplitude, or supercriticality, at which overreflection begins to play a role should be sensitive to the initial horizontal shear in the breaking region, since this controls the width of the region in which the potential vorticity is modified. Also, in agreement with Haynes and McIntyre (1987), the overreflecting solution is sensitive to the inclusion of higher zonal harmonics, whereas in the solutions characterized by absorption, one zonal wavenumber provides a fairly accurate picture of the life cycle.

One obvious limitation of our model is that the vertical resolution is limited to two layers. Since our results qualitatively agree with those from the multilevel primitive equation models, we believe that it is adequate horizontal resolution, not vertical resolution, that is required to see a realistic life cycle. One difference between the high and low vertical resolution models is that in multilevel models the radiating wave can be absorbed at different vertical levels on a critical surface whereas in the present model the radiating wave is absorbed at only one level.

This work can be usefully extended in several directions. The effects of spherical geometry in breaking the symmetry about the jet axis and favoring equatorward propagation are clearly important, but calculations on a β-plane with jets having a north–south asymmetry would also be informative. Would the ratio of the upper layer zonal flow decelerations north and south of the jet depend on supercriticality, for example? Life cycle studies using disturbances with a broader zonal spectrum would also introduce new problems. And the behavior of the forced, dissipative flows must be examined for the more atmospherically relevant case of strong Ekman damping in the lower layer and weak thermal damping.

Acknowledgments. One of the authors (SBF) was supported by NOAA/Princeton University Grant NA87EAD00039.

REFERENCES

Beland, M., 1976: Numerical study of the nonlinear Rossby wave critical level development in a barotropic zonal flow. *J. Atmos. Sci.*, **33**, 2066–2078.

Edmon, H. J., B. J. Hoskins and M. E. McIntyre, 1980: Eliassen–Palm cross sections for the troposphere. *J. Atmos. Sci.*, **37**, 2600–2616.

Geisler, J. E., and R. E. Dickinson, 1974: Numerical study of an

interacting Rossby wave and barotropic zonal flow near a critical level. *J. Atmos. Sci.*, **31**, 946–955.

Haynes, P. H., and M. E. McIntyre, 1987: On the representation of Rossby wave critical layers and wave breaking in zonally truncated models. *J. Atmos. Sci.*, **44**, 2381–2404.

Held, I. M., and B. J. Hoskins, 1985: Large-scale eddies and the general circulation of the troposphere. *Advances in Geophysics*, **28A**, Academic Press, 3–31.

——, and P. J. Phillips, 1987: Linear and nonlinear barotropic decay on the sphere. *J. Atmos. Sci.*, **44**, 200–207.

Killworth, P. D., and M. E. McIntyre, 1985: Do Rossby-wave critical layers absorb, reflect, or over-reflect? *J. Fluid Mech.*, **161**, 449–492.

McIntyre, M. E., and T. N. Palmer, 1984: The "surf zone" in the stratosphere. *J. Atmos. Terr. Phys.*, **46**, 825–849.

Orszag, S. A., 1970: Transform method for calculations of vector-coupled sums: Application to the spectral form of the vorticity equation. *J. Atmos. Sci.*, **27**, 890–895.

Pedlosky, J., 1970: Finite-amplitude baroclinic waves. *J. Atmos. Sci.*, **27**, 15–30.

——, 1971: Finite-amplitude baroclinic waves with small dissipation. *J. Atmos. Sci.*, **28**, 587–597.

——, 1982: Finite-amplitude baroclinic waves at minimum critical shear. *J. Atmos. Sci.*, **39**, 555–562.

——, 1987: *Geophysical Fluid Dynamics*, 2nd ed., Springer-Verlag, 710 pp.

Randel, W. J., and J. L. Stanford, 1985: The observed life cycle of a baroclinic instability. *J. Atmos. Sci.*, **42**, 1364–1373.

Simmons, A. J., and B. J. Hoskins, 1978: The life cycles of some nonlinear baroclinic waves. *J. Atmos. Sci.*, **35**, 414–432.

——, and ——, 1980: Barotropic influences on the growth and decay of non-linear baroclinic waves. *J. Atmos. Sci.*, **37**, 1679–1684.

Smagorinsky, J., 1963: General circulation experiments with the primitive equations: I. The basic experiment. *Mon. Wea. Rev.*, **91**, 99–164.

Warn, T., and H. Warn, 1978: The evolution of a nonlinear critical level. *Stud. Appl. Math.*, **59**, 37–71.

Williams, G. P., 1988: The dynamical range of global circulations—I. *Clim. Dyn.*, **2**, 205–260.